Chapter

Combination of Numerical, Experimental and Digital Image Correlation for Mechanical Characterization of Al$_2$O$_3$/β-TCP Based on CDM Criterion

Barkallah Rachida, Rym Taktak, Noamen Guermazi, Fahmi Zaïri and Jamel Bouaziz

Abstract

Cracks in engineering materials and structures can undergo different modes of deformation. This chapter presents a numerical and experimental approaches aimed to assess the fracture toughness and the Fracture behavior under tensile and shear loading of bioceramics based on commercial Alumina (Al$_2$O$_3$), synthesized Tricalcium phosphate (β-TCP). Conditioning was conducted at different percentages of TCP. After a sintering process at 1600°C for 1 hour, The Crack Straight Through Brazilian Disc were performed by image correlation during a mechanical test and numerical tests were carried out in order to find the angle where the pure mode II. A CDM based constitutive model was selected and implemented into a finite element code to study the damage of our bioceramics. The result of this combination was compared with the direction of crack propagation obtained experimentally. The directions of crack propagation found numerically were found in good agreement with those experimentally obtained by a mechanical test. Alumina-10 wt.% Tricalcium phosphate composites displayed the highest values of the fracture toughness. This value reached 8.76 MPa m$^{1/2}$ MPa. The same optimal composition for the mode I and mode II stress intensity factor with maximum values of 7.6 MPa m$^{1/2}$ and 8.45 MPa m$^{1/2}$ respectively.

Keywords: Fracture, Modeling, Tensile loading, Shear loading

1. Introduction

Recently, the technology of tissue engineering has widely known in substantial advancements and innovations. This technology is a discipline to restoring the task of various organs through the regeneration and also develop novel synthetic biomaterials. It is being investigated and applied in most organ systems, restoring the function of various tissues and organs, such as heart valves, blood vessels and orthopedic implants, among many others [1–3]. Cracks and flaws which certainly exist in the sample reduce in a significant way the load-bearing capacity and then

cause the substitute to break [4, 5]. The fracture toughness and stress intensity factor have been proposed to express the critical stress states in the vicinity of the crack tip, in the aim to analyze crack initiation and propagation [5].

Calcium phosphate bioceramics, with its excellent biological properties, such as biocompatibility and osteconductivity and its outstanding mechanical properties, including hardness, low density and its inertness at high temperature, is widely known as a suitable candidate for biomaterials. Despite their advantages, Calcium phosphates bioceramics exhibit very low toughness which limits their overall applications [6]. The challenge of increasing the toughness of bioceramic has been a key motivation in the field of biomaterials research. In this pursuit of improving toughness, β-tricalcium phosphate (β-Ca3(PO4)2) (β-TCP) are often used due to its outstanding biological responses to physiological environments [7]. The introduction of Alumina (Al2O3) toughening agent increased the toughness of the tricalcium phosphate composite.

Alumina has been widely studied due to its high wear resistance, fracture toughness and strength as well as relatively low friction without forgetting its bioinertness [8].

In recent investigation, Barkallah et al. [9] have been concerned with the Alumina - Tricalcium phosphate composites with different percentages. These Al_2O_3/β-TCP composites have shown a good combination of elastic modulus (76 GPa), tensile strength (27 MPa), compressive (173 MPa) and flexural strength (66 MPa) but this biomaterial has never been investigated the stress intensity factors in Crack Straight Through Brazilian Disc specimen, under tensile and shear loading and their crack's initiation and its propagation. Those parameters of the developed composites should be evaluated.

In fact, there are three basic fracture propagation modes (**Figure 1**): Mode I (opening mode), Mode II (in-plane shear mode), and mixed mode [10]. In pure mode I loading, any two respective points along the notch faces open relative to the notch bi-sector line without any sliding. Under pure mode II, the two respective points along the notch faces slide relative to the notch bi-sector line without any opening and the tangential stress along the bi-sector line is zero. Any combination of mode I and mode II deformation is called mixed mode loading. The shear stress along the bi-sector line is zero for only the loading is pure mode I [11].
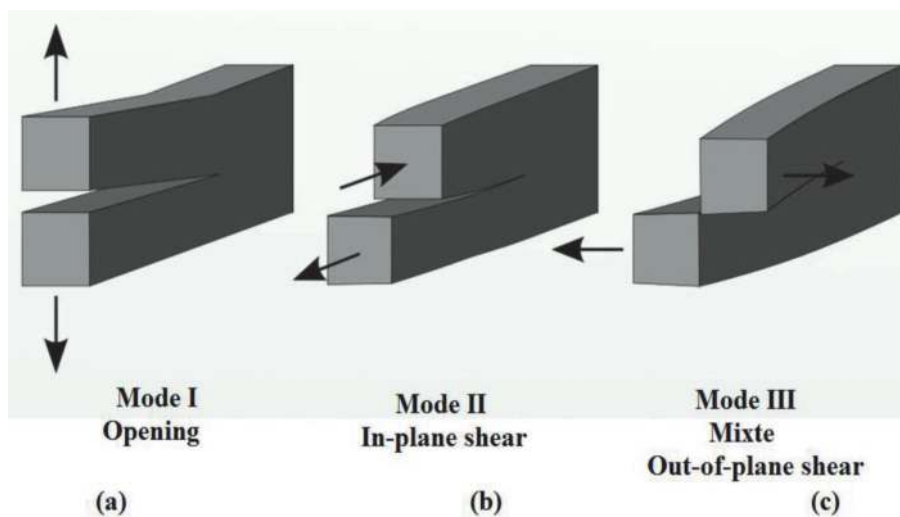

Figure 1.
Basic modes known in fracture mechanics: (a) tensile opening (mode I), (b) In-plane shear (mode II) and (c) out-of-plane shear (mode III).

Many different test specimens have been proposed in the past for brittle or quasi-brittle materials for determining the mode I, II fracture toughness for various engineering materials [12–14]. The centrally cracked Brazilian disc specimen has been used by many researchers to study mode I and mode II fracture mechanics in different brittle materials [11, 14].

Because of the brittleness of Biomaterials based on ceramics, the study of the contact problem with external objects is important. However, ceramics and bioceramics are inherently brittle. This characteristic leads, in particular, to a wide variation in the material strength. A CDM based constitutive model have been developed to study the damage of our bioceramics and thanks to this model, the numerical modeling of the damage behavior of bioceramics during a mechanical test is reported. This modeling is essential for a better understanding of fracture mechanisms of bioceramics [15].

On the other hand, in the last 20 years, digital image correlation (DIC) has shown that it is a valuable non-contact technique for measuring kinematic fields during a mechanical test [16, 17]. In order to account for the maximum load, it is crucial to work with local displacements at the damage progress zone.

In this chapter, we present a damage model in combination with finite element technique that can help automatize the damage progress fracture in an efficient manner. Our work was undertaken to evaluate the mechanical behavior of the combination of commercial alumina with synthetic Tricalcium phosphate as bone substitute material. To achieve this purpose, we study the stress intensity factor KI under tensile stress (mode I rupture) and stress intensity factor KII under shear stress (mode II rupture experimentally and theoretically using modified Brazilian test. The samples were also characterized by scanning electron microscopy (SEM).

2. Materials and methods

2.1 Materials

In order to elaborate Al_2O_3-TCP, the materials used were commercial Al_2O_3 (Riedel-de Haën, purity >98%) and synthesized tricalcium phosphate powders.

The β-TCP powder was synthesized by solid-state reaction from calcium phosphate dibasic anhydrous ($CaHPO_4$) and calcium carbonate ($CaCO_3$). Stoichiometric amounts of high purity powders, $CaCO_3$ (Fluka, purity ≥98.5%) and $CaHPO_4$ (Fluka, purity ≥99%) were sintered at 1000°C for 20 hours to obtain the β-TCP according to the following reaction [18]:

Synthesized Tricalcium phosphate was introduced with α-Alumina powders. The approximate representatives Al_2O_3-TCP were {90 wt.%, 10 wt.%}, {80 wt.%, 20 wt.%}, {60 wt.%, 40 wt.%} and {50 wt.%, 50 wt.%}.

It is worth mentioning that the size of particles of each powder was measured (2.53 μm for Al_2O_3 and 2.79 μm for TCP).

As starting materials, calculated quantities of The β-TCP and Al_2O_3 powder were mixed by homogeneous mixing in a mortar and milled in absolute ethanol and treated with an ultrasound machine for 20 min. After milling these powders, the mixture was dried at 80°C for 24 hours to eliminate the ethanol. After drying, mixtures powders thus prepared were molded in a metallic cylinder mold having a diameter of 30 mm and a thickness of 5 mm and uniaxially pressed at 67 MPa. A crack "2a" of 12 mm was added to the CSTBD specimens were considered for each compacted specimens. The crack of the CSTBD specimens was added by a specific metal mold (**Figure 1**). At least six specimens were tested under each test condition.

Finally, the specimens were sintered at 1600°C for 1 hour in a vertical program-mable muffle furnace (Pyrox 2408) and were heated and cooled at a rate of 10° C min^{-1} and 20°C min^{-1}, respectively.

On the other hand, one side of each fracture sample has been sprayed with black then white paint in order to form the speckle pattern that will be used by the Digital Image Correlation (DIC) technique.

2.2 Experimental part

At least six specimens were tested under each condition and then average values (K_{IC}, K_I and K_{II}) were considered.

2.2.1 Bending test.

The fracture toughness K_{IC} of the samples were assessed using Semi Circular Bending tests. The samples were positioned on the loading platform by 3-point compressive loading, at a uniform loading speed of 0.075 mm/min (**Figure 2a**). The SCB specimen diameter is equal to 30 mm and 5 mm for thickness. The specimen contains a crack of 4 mm in the semi disc, as shown in **Figure 2b**. The crack-length-to diameter ratio S/D was 0.13.

Using the SCB specimen with straight crack, the fracture toughness K_{IC} was calculated with the following formula [19]:

$$K_{IC} = \frac{P_{max}\sqrt{\pi a}}{2Rt} Y_I(a/R, S/R) \qquad (1)$$

Where a is the crack length, P_{max} is the maximum load, D is the cylindrical block diameter and YI is the geometry factor. The latter is a function of the ratio of the crack length (a) over the semi-disc radius (R) and the ratio of the half-distance between the two bottom supports (S) over the semi-disc radius (R) (**Figure 2b**). The geometry factor Y_I is expressed as follows [19]:
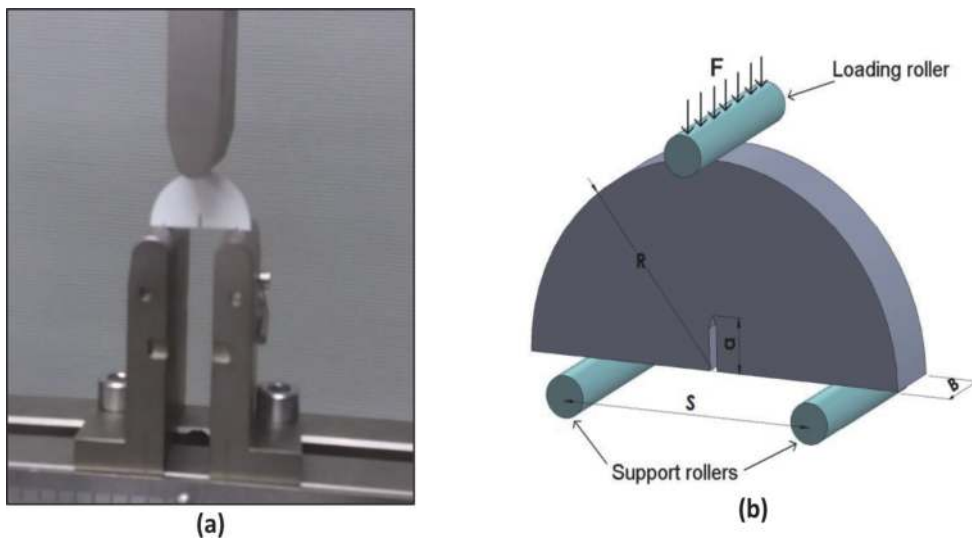

(a)   (b)

Figure 2.
Semi-circular bending (SCB): (a) real photo of SCB test (b) illustration of cracked SCB specimen.

$$Y_I(a/R, S/R) = \frac{S}{R}\left(2.91 + 54.39\frac{a}{R} + 391.4\left(\frac{a}{R}\right)^2 + 1210.6\left(\frac{a}{R}\right)^3 - 1650\left(\frac{a}{R}\right)^4 + 875\left(\frac{a}{R}\right)^5\right)$$

$$(2)$$

2.2.2 Cracked straight-through Brazilian disc

The introduction of the fracture mechanics approach to brittle materials has led to the development of materials fracture mechanics, which refers to the initiation and propagation of a crack or many cracks in materials.

According to the applied stress condition, a crack propagates depending on the three basic failure modes [20]: Mode I loading state is defined as opening mode, the mode II is defined as sliding mode (shear mode) and mode III is defined as tearing.

In this chapter, only mode I and II will be studied and detailed. Bioceramic stress intensity factor under modes I and II was measured using CSTBD specimens for an experimental and analytical investigation [21, 22]. Disc-type specimens are simple in geometry and have many advantages in terms of sample preparation, testing and analysis.

Different combinations of mode I and mode II can be shown by changing the crack angle β: if the direction of compressive applied load is along the crack bi-sector line β = 0, the samples is subjected to pure mode I loading. If β ≠ 0, the samples are subjected to mixed mode I/II loading. A gradual increase of the loading angle results in an elevation in mode II effects and reduction in mode I effects. Finally, there are a specific loading angle β_II for which the sample undergoes pure mode II deformation. This angle was found in this research by a series of finite element analyses [11].

The UMTS criterion is a criterion for brittle fracture is proposed by Ayatollahi [11] for prediction the mode II fracture toughness of U notched components and the fracture initiation angle in CSTBD under pure mode II loading.

The International Society for Rock Mechanics (ISRM) proposed many analytical formulas for measuring fracture toughness mode I of brittle materials: the cracked chevron notched Brazilian disc (CCNBD) specimens and the Cracked straight through Brazilian disc (CSTBD) [12, 23] (see **Figure 3a** and **b**). The CSTBD and CCNBD specimens has the same geometry and shape as the conventional Brazilian disc used for measuring the indirect tensile strength, except that the CSTBD specimen has a through notch length of 2a, by means of the straight-through crack assumption (STCA) method.

By comparing these two methods, CSTBD has superiority over CCNBD considering that producing a stream crack is easier than a V-shape crack. [14, 24]
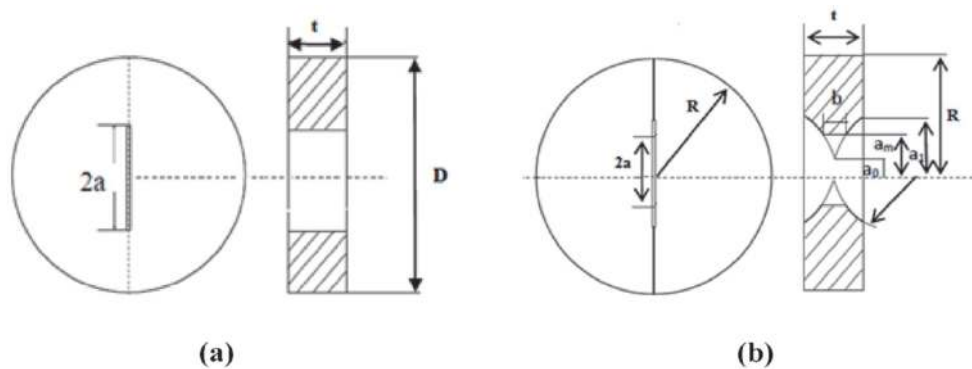

(a)   **(b)**

Figure 3.
Disc-type specimens: (a) CSTBD and (b) CCNBD.

The stress intensity factor (SIF) solutions for CSTBD specimens can be met in Cherepanov's book [25] and the handbook [26]. the main formulas to remember are collected as follows:

Cherepanov's book:

$$K_I = \frac{P}{\sqrt{D}\, t}\, Y \tag{3}$$

$$Y = \sqrt{\frac{2}{\pi}}\sqrt{\alpha}\left[1 + \frac{3}{2}\alpha^2 + \frac{3}{4}\alpha^6 + \frac{3}{64}\alpha^8\right] \tag{4}$$

The handbook:

$$K_I = \frac{P}{\sqrt{D}\, t}\, Y \tag{5}$$

$$Y = \sqrt{\frac{2}{\pi}}\sqrt{\frac{\alpha}{1-\alpha}}\left[1 - 0.4964\,\alpha + 1.5582\,\alpha^2 - 3.1818\,\alpha^3 + 10.096\,\alpha^4 - 20.7782\,\alpha^5\right.$$
$$\left. + 20.1342\,\alpha^6 - 7.5067\,\alpha^7\right] \tag{6}$$

where $\alpha = \frac{a}{R}$ knowing that K_I is the mode-I stress intensity factor, Y is the dimensionless stress intensity factor, P is the concentrated diametral compressive load, D is the diameter, t is the thickness and a is the crack length.

According to [27], the analytical solution of the stress intensity factor SIF for the CSTBD specimen for measuring the fracture toughness of ceramics can be expressed in the following form Shetty et al. [28]:

$$K_I = \frac{P}{\pi\,R\,t}\sqrt{\pi\,a}N_I = \frac{P}{\sqrt{\pi}\,R\,t}\sqrt{\alpha}N_I \tag{7}$$

Where P is the load applied in compression, a is half the notch length and N_I is the dimensionless stress intensity factor depending on the dimension less crack length α (a/R) and the notch inclination β.

N_I solutions for the CSTBD sample can be determined by several methods:

Starting with Atkinson et al. [29] who has developed N_I solutions for determining the fracture toughness and applied the stress intensity factor solutions of the CSTBD.

By small crack approximation ($\alpha \le 0.3$) and five-term approximation, N_I was developed as the following formula:

$$\boldsymbol{N_I} = 1 - 4\,sin^2\beta + 4\,sin^2\beta(1 - 4\,cos^2\theta)\alpha^2 \tag{8}$$

With

$$\alpha = \frac{a}{R}$$

when β = 0, the problem is reduced to theMode I fracture situation, then according to, the previously equation $\boldsymbol{N_I}$ becomes [28]:

$$\boldsymbol{N_I} = 0.991 + 0.141\,\alpha + 0.863\,\alpha^2 + 0.886\,\alpha^3 \tag{9}$$

Wherever, Fowell et al. [22] developed the formula on other form $0.05 \leq \alpha \leq 0.95$:

$$
\begin{aligned}
N_I = \sqrt{\frac{\pi}{\alpha}}\big(&0.0354 + 2.0394\,\alpha - 7.0356\,\alpha^2 + 12.1854\,\alpha^3 + 8.4111\,\alpha^4 - 30.7418\alpha^5 \\
&- 29.4959\,\alpha^6 + 62.9739\,\alpha^7 + 66.5439\,\alpha^8 - 82.1339\,\alpha^9 - 73.6742\,\alpha^{10} \\
&+ 73.8466\,\alpha^{11}\big)
\end{aligned}
$$

$$(10)$$

As mentioned, different combinations of mode fracture can be obtained by changing the angle β. For while mode II, we can find the specific loading angle β, for which the specimen undergoes pure mode II deformation, by a series of finite element analyses. The mode II loading angle β was then determined from finite element results for the notch length that is already selected for mode I.

The stress intensity factor, for the CSTBD specimen with a through notch length of 2a, under mode II can be calculated with the following formula [28]:

$$
K_{II} = \frac{P}{\pi R t}\sqrt{\pi a}N_{II} = \frac{P}{\sqrt{\pi R t}}\sqrt{\alpha}N_{II}
\tag{11}
$$

$$
N_{II} = \big[2 + (8\cos^2\theta - 5)\alpha^2\big]\sin 2\beta
\tag{12}
$$

Where P is the load applied in compression, a is half the crack length and N_{II} is the dimensionless stress intensity factor under mode II, depending on the dimensionless notch length $\alpha = a/R$ and the crack inclination angle with respect to loading direction, β (**Figure 4**).

In this case, N_{II} was developed by [29].

2.2.3 Digital correlation

Nowadays, various full-field non-contact optical methods have been reported in literature and succeeded in replacing those classical techniques by Digital image correlation for strain and displacement measurements [16, 30]. The principle of DIC analysis is based on the comparison of the different successive digital images acquired during the test.
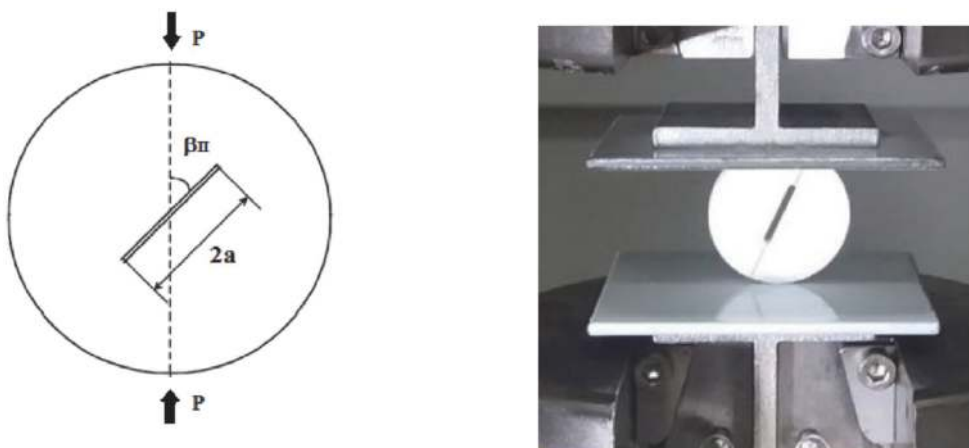

Figure 4.
CSTBD under pure mode II fracture.

As mentioned in introduction, the experimental displacement was here computed by using Digital Image Correlation (DIC) in order to determinate the crack propagation at different states of loading and different composition. In the present work, DIC calculations have been managed with Correla software.

At each load step and at each composition, a series of images is taken with a CCD camera and digitalized and then compared to the reference image. For this technique, the displacement field analysis was performed inside of a Region of Interest (ROI) divided into discrete subsets. The shape (square or rectangular), the size (number of pixels) and the distribution (vertical and horizontal distances between centres, (Lx,Ly)) of these subsets should be carefully chosen. Those parameters depending to the desired accuracy of measurements (displacement and strain) and to the spatial resolution for map fields [16].

For each subset, a correlation function is used to estimate the degree of similarity between the reference image state and the current one (for each given load) [31].

Increasing the sub-set size allows decreasing the uncertainty because DIC error mainly depends on the number of pixels in thesubset [17]. The dedicated subsets were voluntary chosen with different scale factor (as shown on **Table 1**).

2.3 CDM model

In this study, the FE simulations were performed by a constitutive model describing the mechanical behavior of brittle material is based on the CDM approach.

At first, The CDM approach was introduced by Kachanov [32] and generalized later by Le maitre and Chaboche [33]. It is a concept which provides a mathematical description of the effect of micro-defects and micro-cracks, at a macro-scale, on the macroscopic properties of the material. After that, the works of J. Ismail [15] show that even the mathematical formulation of this damage mechanics model that allows it to predict the cracking damage patterns in brittle materials.

Composition	Scalor factor (mm/pixel)
Alumine	0,047138
Al_2O_3–10 wt.% TCP	0,047138
Al_2O_3–20 wt.% TCP	0,0474517
Al_2O_3–40 wt.% TCP	0,0470807
Al_2O_3–50 wt.% TCP	0,0480663
Al_2O_3–10 wt.% TCP - 1 wt.% TiO_2	0,04803
Al_2O_3–10 wt.% TCP - 2,5 wt.% TiO_2	0,04803
Al_2O_3–10 wt.% TCP - 3 wt.% TiO_2	0,0481132
Al_2O_3–10 wt.% TCP - 4 wt.% TiO_2	0,048955
Al_2O_3–10 wt.% TCP - 5 wt.% TiO_2	0,0480843
Al_2O_3–10 wt.% TCP - 7,5 wt.% TiO_2	0,0481766
Al_2O_3–10 wt.% TCP - 10 wt.% TiO_2	0,0481766

Table 1.
Calibration scalor factor.

For an exact estimation of damage patterns, there is a clear need of constitutive equation of brittle material that is defined by:

$$\sigma = k * \varepsilon \tag{13}$$

where K is the fourth-order stiffness tensor which is written as

$$k = k^e + k^d \tag{14}$$

in which k^e denotes the fourth-order stiffness tensor for the isotropic virgin material. k^d is a fourth-order tensor which represents the added damage influence and the final expression is given by

$$k^d_{ijkl} = C1 \left(\delta_{ij} D_{kl} + \delta_{kl} D_{ij} \right) + C2 \left(\delta_{jk} D_{il} + \delta_{il} D_{jk} \right) \tag{15}$$

where δ is the Kronecker-delta symbol and C1 and C2 are the damage parameters.

The damage variables that expressed as functions of stress state is introduced into an anisotropic damage tensor D_{ij}. Their values vary between 0 for virgin state and 1 for fully damaged (cracking) state.

Both damage patterns (mode I/mode II) are modeled by taking into consideration the effects of tensile principal stresses as well as compressive and shear stresses.

For the functioning of damage tensor, account should be taken of the effect of normal principal stress and those shear stress components in the damage mechanisms in brittle materials and the damage for both modes I and II is modeled.

- The first types of components (mode I)

This mode is involved by normal tensile principal stresses. The damage components representing are the diagonal terms of tensor K and their values are expressed in term of critical and threshold stress limits by:

.1

$$D_{ii} = \begin{cases} 0 \ if \ \sigma_i \leq \sigma_t \\ \dfrac{\sigma_i - \sigma_t}{\sigma_c - \sigma_t} \ if \ \sigma_t < \sigma_i < \sigma_c \ \ i = 1, 2, 3 \\ 1 \ if \ \sigma_i \geq \sigma_c \end{cases} \tag{16}$$

Where σ_c and σ_t are the critical and threshold stresses that corresponds to the stress below which no damage occurs.

- The second types of components (mode II)

In some cases, the shear mode (mode II) could be activated. Those components are formulated as a function of shear stress in the symmetry plane. The general form is:

$$D_{ij} = \begin{cases} 0 & \text{if } \sigma_{ij} \leq \tau_t \text{ and } \max(\sigma_i) > 0 \\ \dfrac{\sigma_{ij} - \tau_t}{\tau_c - \tau_t} & \text{if } \tau_t < \sigma_{ij} < \tau_c \text{ and } \max(\sigma_i) < 0 \\ 1 & \text{if } \sigma_{ij} \geq \tau_c \text{ and } \max(\sigma_i) > 0 \end{cases} \tag{17}$$

$$i = 1, 2, 3 \text{ and } i \neq j$$

Where τ_c and τ_t are the critical and threshold shear parameters, respectively.

The damaged constitutive equations were coded in the Fortran programming language and implemented in the commercial FE code MSC. Marc to simulate the behavior and damage evolution in our materials.

The micro-cracks and micro-defects are an irreversible phenomenon. For this reason, the damage does not decrease during the loading and the D_{ij} is taken as a monotonic increasing function of time increment:

$$D_{ij} = \max\left(D_{ij}^n, D_{ij}^{n-1}\right) \tag{18}$$

Where D_{ij}^n is the damage value at the current time step n and D_{ij}^{n-1} is the damage value at the previous time increment n-1.

A procedure to identify the model parameters must now be defined. The input parameters required are:

- The Poisson's ratio

- The Young's modulus

- The critical and threshold stresses: c and t in mode I.

- The breaking load

The material properties such as the ultimate tensile strength (σ_t), the elastic modulus (E) and the Poisson's ratio (μ) for Al_2O_3-TCP were determined experimentally using the standard test techniques at room temperature.

2.4 Finite element analysis

In this section, the commercial FE code MSC. Marc was used to perform the simulations. A two-dimensional calculation has been performed using the finite element program MARC. A plane stress FE model with a total number of 8000 Quad 4 elements was created for simulating the specimen by moving two plates to effect compression on the disk. **Figure 5a** shows a sample FE grid pattern used for simulating a CSTBD specimen. The finest elements were located near the notch tip due to its high stress gradient (**Figure 5b**).

In order to determine the angle β_{II} for which the sample undergoes pure mode II deformation, this angle was found in this research by a series of finite element analyses. Then, the values of the tangential and the shear stresses (σ_{12}, σ_{22}) along the notch bi-sector line could be obtained from the FE results In a Cartesian coordinate. In an auxiliary system of curvilinear coordinates, when $\sigma_{\theta\theta}(r_0, 0) = 0$, the mode I is zero, and hence the specimen is subjected to pure mode II deformation. Therefore, the mode II loading angle β_{II} is the angle for which $\sigma_{\theta\theta}(r_0, 0) = 0$ [11].
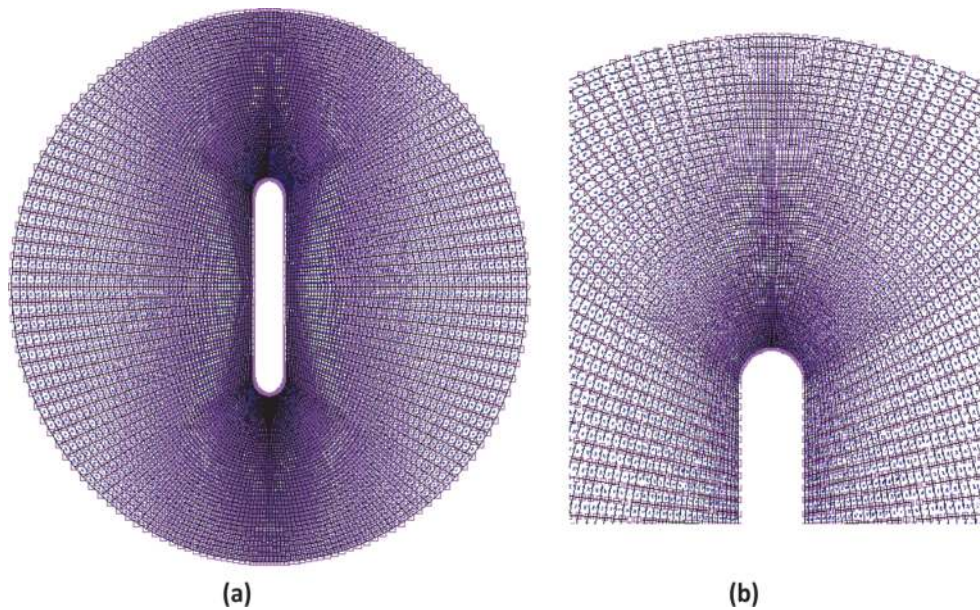
Figure 5.
A FE grid used for the simulations: (a) FE-mesh for the whole sample, (b) FE-mesh near the notch tip.

After having used the matrix for passing from a Cartesian coordinate system to a cylindrical coordinate system, $\sigma_{\theta\theta}$ can write Eq. (19),

$$\sigma_{\theta\theta} = \sigma_{22} * \cos(\theta) - \sin(\theta) * \sigma_{12} \qquad (19)$$

In order to obtain the pure mode II loading angle β_{II}, the angle b was gradually increased from zero and the value of tangential stress $\sigma_{\theta\theta}(r_0, 0)$ at the notch tip was calculated for each loading angle, under a compressive load already found by the mechanical tests. As the loading angle increased, the value of $\sigma_{\theta\theta}(r_0, 0)$ decreased until it was equal to zero.

In a second step, a CDM criterion for brittle materials has been introduced in the MARC-2005 to predict the mechanical behavior of our biomaterials subjected to a mechanicals test and this modeling was used to simulate the damage process. This combination has allowed to detect crack initiation and to analyze fracture process.

The mechanical properties were chosen to represent the composite specimens, for which elastic modulus and Poisson's ratio are (47.03; 75.96; 55.75; 46.86 and 33.51 GPa) and (0.283; 0.318; 0.361; 0.363 and 0.28), respectively for the variation of TCP.

3. Results and discussion

3.1 Determination of β under mode II

The CSTBD specimen has been used by many researchers to study mode I and mode II brittle fracture in different materials. However, the experimental results obtained in the past part from this specimen indicate that the mode II is β = 22° [34] and β = 25° [11].

Depending on the crack length and the disc radius already chosen, the numerical calculation reported in this figure (**Figure 6**) shows that the stress (σ) is equal to zero near to angle 22, this result is similar for all compositions, so this angle verifies the pure mode II. Therefore, the results of the FE analysis have been obtained shows
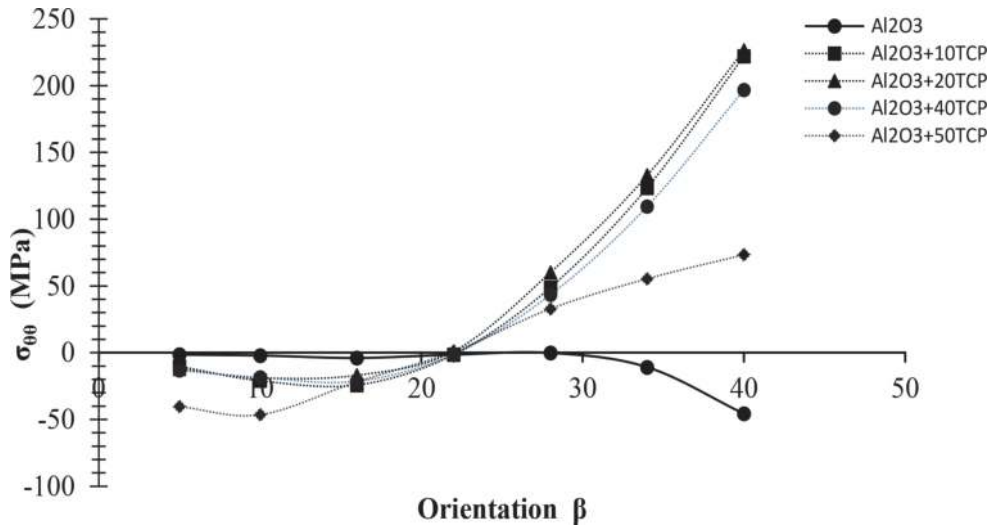
Figure 6.
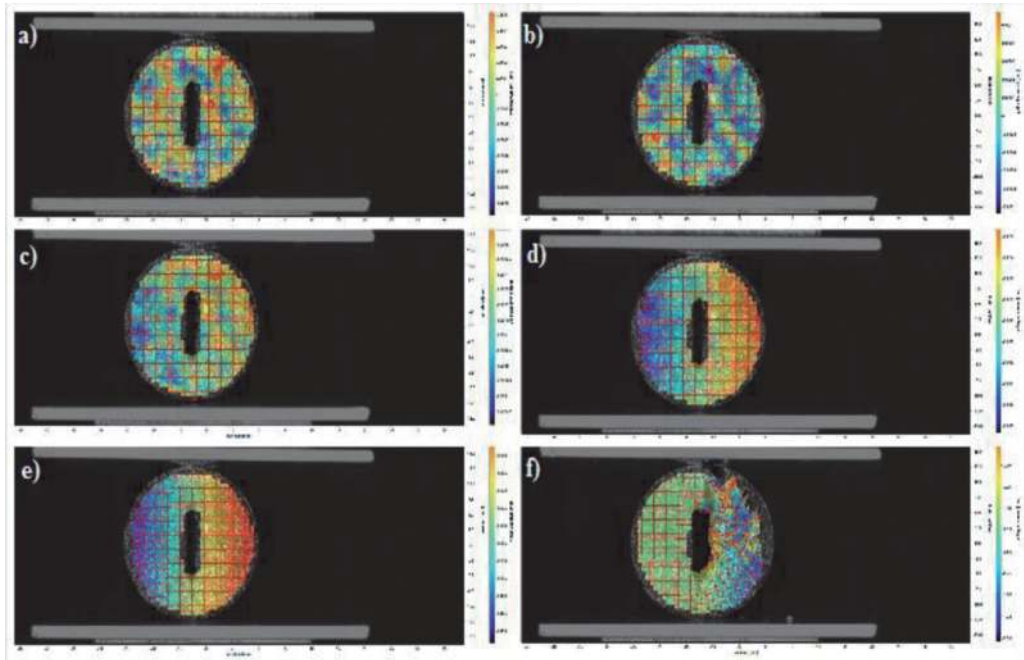*Variation of $\sigma_{\theta\theta}$ for each compositions.*

Figure 7.
The image of correlation.

that the angle 22°C verifies the pure mode II. The value of this angle is in the interval of 20° and 30°. A very good agreement is shown between the theoretical predictions and the experimental results. Applying the load, the same crack propagation is carried out in the numerical and experimental element.

3.2 Digital image correlation

For mode I, a series of images is taken with a CCD camera and digitalized and then compared to the reference image. It has been verified that in Mode I loading, the crack surfaces separate symmetrically and the crack front propagates in the direction of the crack plane (**Figure 7**).

3.3 Determination of stress intensity factor under mode I

Since the CSTBD specimen is closely linked to fracture toughness and stress intensity factor, this sub section is there for compare different solutions of stress intensity factor under mode I. We used the experimental data of the CSTBD samples to define KI, by applying the previous formulas Eq. (3) using two different term of Y (6) and Eq. (7) using the different term of dimensionless stress intensity factor (NI) (9) and (10), for different percentages of TCP additive calculation is launched for crack length a/R = 0.4.

According to our previously work [9], the used composite specimens reached their optimum in mechanical properties at 1600° C. **Figure 8** illustrates the evolution of the stress intensity factor under mode I fracture in relation to the percentage of TCP under optimal conditions at 1600°C for 1 hour using different methods. We note that the Cherepanov, SIF values are close to those by handbook, Shetty and Fowel and al. Hence, K_I (Cherepanov) is basically consistent with K_I (handbook) and K_I (Shetty et all) and shows a good compromise in the results.

For the study of the effect of TCP, this figure has illustrated that the stress intensity factor K_I increases with the addition of 10 wt.% of TCP until 8.452 MPa m$^{1/2}$ using the formula mentioned in Cherepanov's book. Beyond this percentage of TCP, the overall stiffness falls gradually.

The initiation and propagation of each crack depends on the type of solicitation. According to this test condition, cracks propagates in a parallel manner to the direction of the notch, and as soon as it intersects with the surface, the sample is divided into two parts. These cracks are generated by principal stresses, under mode I loading (As shown in **Figure 9**).

3.4 Determination of stress intensity factor under mode II

In this research, the loading angle corresponding to mode II deformation in the CSTBD specimens is approximately equal to 22 (deg.) for α = 0.4. Consequently, the mode II fracture tests were performed according to these loading angle and then K_{II} is determined for pure mode II. In this test condition, a crack propagates according
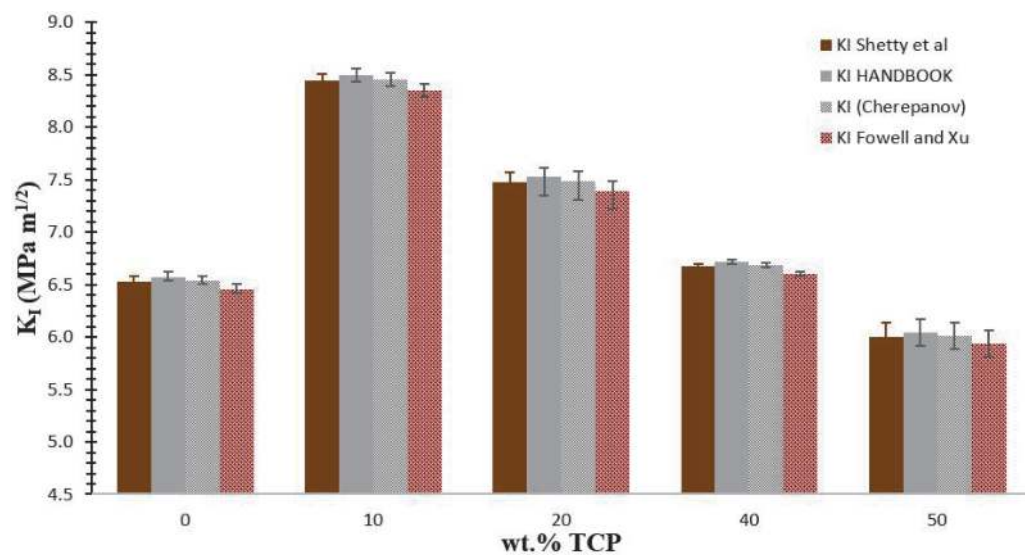

Figure 8.
Mode I stress intensity factor versus percentage of TCP additive in Al2O3 using different methods.
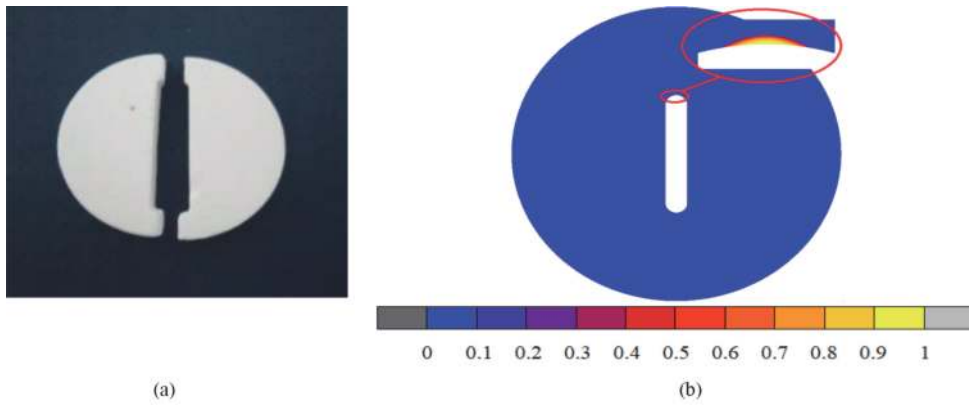
Figure 9.
Influence of mode I (opening mode) on crack initiation and propagation after the fracture tests:
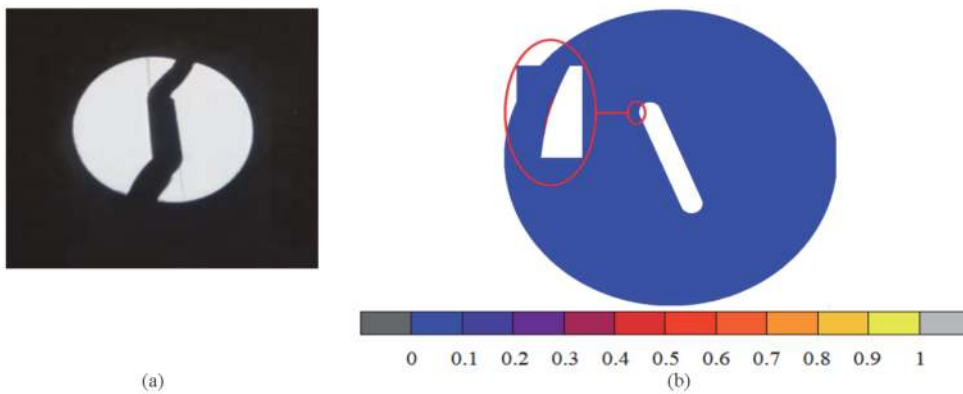*(a) experimental fracture and (b) numerical fracture.*

Figure 10.
Influence of mode II (shearing mode) on crack initiation and propagation after the fracture tests: (a)
experimental fracture and (b) numerical detection by successive simulations of the mode II loading angle
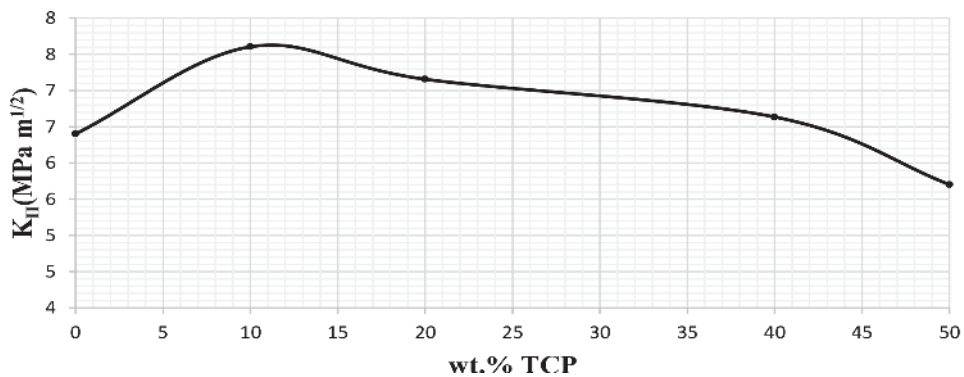*resulting in pure shearing mode effects.*

Figure 11.
Mode II stress intensity factor versus percentage of TCP additive (in Al_2O_3).

to mode II test and the same crack propagation is carried out in the numerical and experimental part. (see **Figure 10**).

Analytical analysis for this geometry is accomplished by using Eq. (11). **Figure 11** presents the test results for the calculation of the stress intensity factor for the same crack length with different percentages of TCP respectively. The stress

intensity factor mode II fracture values of Al_2O_3-wt.% TCP composites are comprised between 5.8 MPa m$^{1/2}$ and 7.6 MPa m$^{1/2}$. The lowest toughness is obtained with the 50 wt.% TCP, while the highest one is approached with the 10 wt.% TCP (7.6 MPa m$^{1/2}$) (see **Figure 11**).

3.5 Determination of the fracture toughness K_{IC}

For the SCB test, after the crack starts from the disc center at the maximum load, the crack propagates symmetrically ahead the loading diameter. K_{IC} is determined by applying Eq. (1), the K_{IC} is calculated for different percentages of TCP.

Figure 12 shows the fracture toughness of different amounts of TCP added to Alumina. As sintered at 1600°C/1 h, The best value of the fracture toughness value of Al_2O_3/10 wt.% TCP composites is 8.76 MPa m$^{1/2}$.

3.6 S.E.M characterization of sintered samples

The microstructure of the sintered specimens was observed by scanning electronic microscopy (SEM). **Figure 13** shows the S.E.M micrographs of the Alumina (Al_2O_3) reinforced with the Tricalcium phosphate (TCP) with different additives amounts sintered at 1600°C for 1 hour. This technique helps to investigate the porosity and the texture of any biomaterial. These micrographs show the coalescence between alumina grains produced with all the percentages of added TCP (**Figure 13(a–f)**).

These micrographs show the difference between fracture surface of Alumina, Alumina −10 wt.% TCP and Alumina −50 wt.% TCP samples (**Figure 13(a–f)**). The SEM micrographs of the pure Alumina sintered without TCP show an intergranular porosity (**Figure 13a** and **b**). The significant improvement of the characteristics of the Al_2O_3–10 wt.% TCP samples can be explaining by a coalescence between Alumina grains produced with all the percentages of added TCP. In addition, the formed spherical pores demonstrate that a liquid phase was formed a 1600°C (**Figure 13c** and **d**). For this composition, one notices also the absence of micro-cracking and the reduction of the sizes of the pores that achieves higher
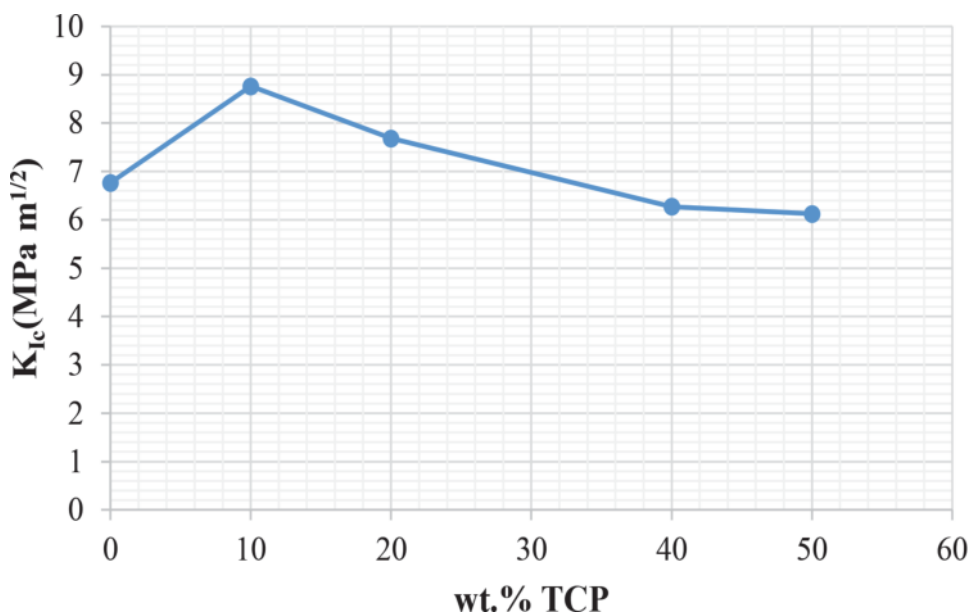

Figure 12.
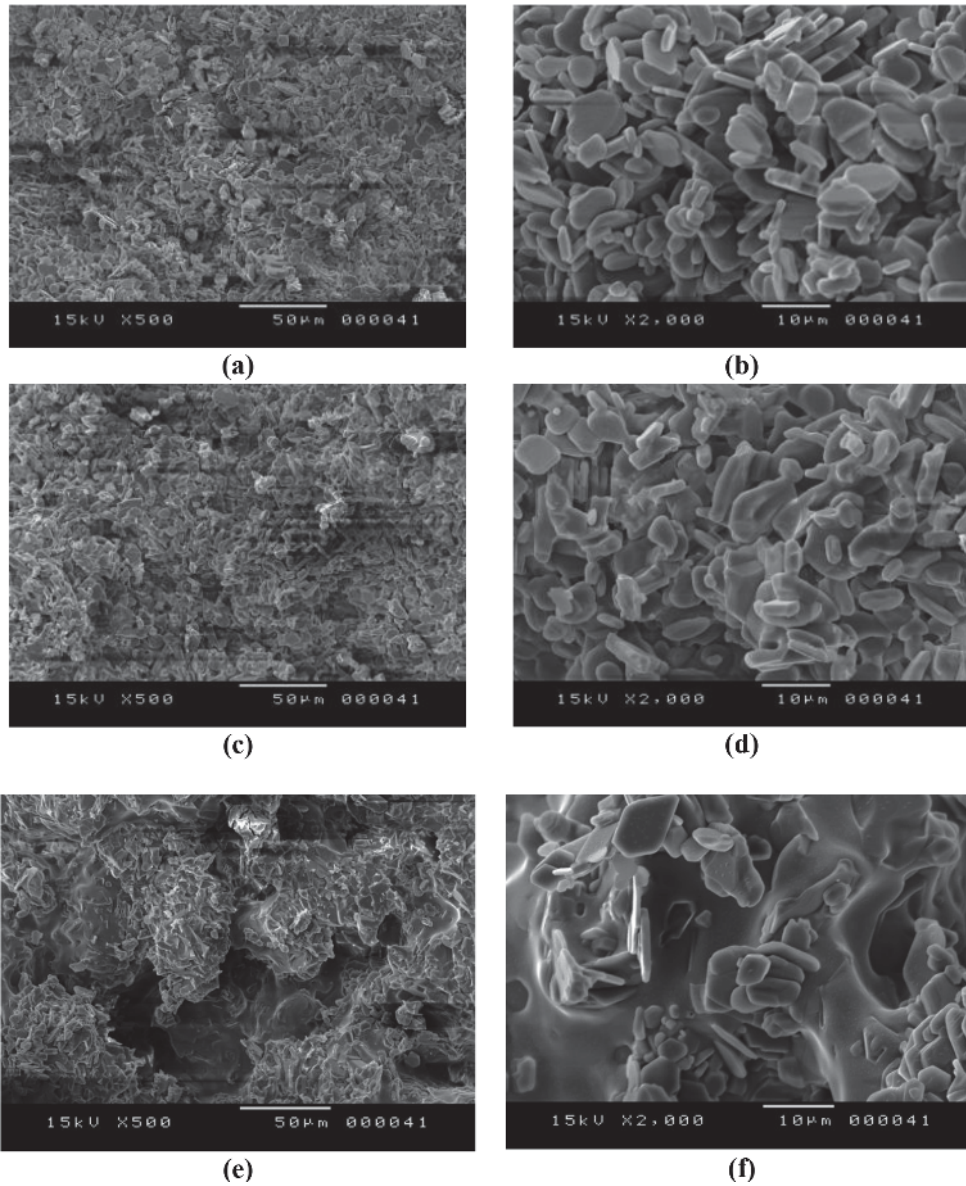*Fracture toughness (K_{IC}) as function of the percentage of TCP.*

Figure 13.
SEM micrographs of different bioceramic composites sintered at 1600°C for 1 h: (a) and (b) Al_2O_3, (c) and (d) Al_2O_3–10 wt.% TCP, (e) and (f) Al_2O_3–50 wt.% TCP.

densities and decrease the grain size. For this reason, the Alumina-10 wt.% TCP composite presents excellent mechanical properties.

The strength started to decrease with higher percentage of TCP (20, 40, and 50 wt.%). A particular relation between grain size and mechanical strength in sintered alumina-TCP composites was found.

4. Conclusion

This work aimed at studying the fracture behavior of the Alumina-Tricalcium phosphate. From the main results, the following conclusions can be drawn:

The fracture toughness KIC of the samples contains a crack were assessed using Semi Circular Bending tests. The best fracture properties in terms of fracture

toughness, were obtained for Al2O3–10 wt.% TCP composition. The best value is 8.76 MPa m$^{1/2}$.

The CSTBD specimen is an appropriate test specimen for fracture tests of U-shaped notches particularly when the notch is subjected to pure mode II loading.

The CSTBD specimen was employed for mixed Mode I and II fracture studies. The numerical analysis of Alumina-TCP subjected to static indentation by a spherical indenter was presented. From a CDM based constitutive modeling, the anisotropic damage mechanisms developed in the specimens were examined through the principal (mode I) and shear stresses (mode II). The stress intensity factor under mode I and II of the Alumina-TCP composites increase with the amount of TCP until 10 wt.%.

The initiation and propagation of each crack depends on the type of solicitation. The geometry model used includes a Brazilian disc containing a crack with two different orientations: 0° for tensile mode (mode I), 22° for shear mode (mode II). The predicted directions were found in good agreement with the experimental observations reported in the literature.

Author details

Barkallah Rachida[1]*, Rym Taktak[1], Noamen Guermazi[2], Fahmi Zaïri[3] and Jamel Bouaziz[1]

1 Laboratoire des MatériauxAvancés (LMA), EcoleNationaled'Ingénieurs de Sfax (ENIS), Université de Sfax, Tunisia

2 Laboratoire de Génie des Matériaux et Environnement (LGME), Ecole Nationale d'Ingénieurs de Sfax (ENIS), Université de Sfax, Tunisia

3 Lille University, Civil Engineering and Geo-Environmental Laboratory (ULR 4515 LGCgE), Lille, France

*Address all correspondence to: barkallah_rachida1@live.fr

IntechOpen

References

[1] Zeineddine Hussein A, Frush Todd J, Saleh Zeina M, et al. Applications of tissue engineering in joint arthroplasty: current concepts update. Orthopedic Clinics. 2017; 48(3): 275-288. doi: 10.1016/j.ocl.2017.03.002.

[2] Shin YS, Choi JW, Park JK, et al. Tissue-engineered tracheal reconstruction using mesenchymal stem cells seeded on a porcine cartilage powder scaffold. Ann Biomed Eng. 2015;43(4):1003–13. DOI: 10.1007/s10439-014-1126-1

[3] Sun H, Liu W, Zhou G, et al. Tissue engineering of cartilage, tendon and bone. Frontiers of medicine. 2011;5(1): 61–9.https://doi.org/10.1007/s11684-011-0122-1

[4] Ayatollahi MR, Aliha MRM, Saghafi H. An improved semicircular bend specimen for investigating mixed mode brittle fracture. EngFract Mech. 2011;78(1):110–123. doi.org/10.1016/j.engfracmech.2010.10.001 11.

[5] XIE, Yousheng, CAO, Ping, JIN, Jin, et al. Mixed mode fracture analysis of semi-circular bend (SCB) specimen: a numerical study based on extended finite element method. Computers and Geotechnics. 2017;82:157–172.https://doi.org/10.1016/j.compgeo.2016.10.012

[6] AYADI Ibticem, AYED Foued Ben. Sintering and the mechanical properties of the tricalcium phosphate–titania composites. journal of the mechanical behavior of biomedical materials. 2015; 49:129-140.DOI: 10.1016/j.jmbbm.2015.05.001

[7] R D AGaasbeek, H G Toonen, RJ Van Heerwaarden, P Buma, Mechanism of bone incorporation of β-TCP bone substitute in open wedge tibial osteotomy in patients. Biomaterials. 2005; 26:6713–6719.DOI: 10.1016/j.biomaterials.2005.04.056

[8] J.L. Runyan, S.J. Bennison, Fabrication of flaw-tolerant aluminiumtitanate-reinforced alumina, J. Eur. Ceram. Soc. 7 (1991) 93–99.https://doi.org/10.1016/0955-2219(91)90006-L

[9] RBarkallah, RTaktak, NGuermazi, FZaïri, JBouaziz, FZaïri. Manufacturing and mechanical characterization of Al2O3/β-TCP/TiO2 biocomposite as a potential bone substitute. Int J AdvManuf Technol. 2017; 3369–3380. DOI:10.1007/s00170-017-1434-3

[10] YAO Wei, XU Ying, YUChangyiet al. A dynamic punch-through shear method for determining dynamic Mode II fracture toughness of rocks. Engineering Fracture Mechanics. 2017; 176: 161-177. https://doi.org/10.1016/j.engfracmech.2017.03.012

[11] AyatollahiM R, Torabi A R. Determination of mode II fracture toughness for U-shaped notches using Brazilian disc specimen. International Journal of Solids and Structures. 2010; vol. 47, no 3-4, p. 454-465. https://doi.org/10.1016/j.ijsolstr.2009.10.012

[12] QZ Wang, Formula for calculating the critical stress intensity factor in rock fracture toughness tests using cracked chevron notched Brazilian disc (CCNBD) specimens, Int JRock Mech Min Sci. 2010; 47:1006–1011. DOI: 10.1016/j.ijrmms.2010.05.005

[13] SH Chang, CLee, S Jeon, Measurement of rock fracture toughness under modes I and II and mixed-mode conditions by using disc-type specimens. Eng. Geol. 2002; 66:79–97. DOI:10.1016/S0013-7952(02)00033-9

[14] Ghavidel NA, Memarian H, Mohamadi S, Heydarizadeh M. Analytical Solution for Stress Field and Intensity Factor in CSTBD under Mixed Mode Conditions, Int. J. Min. & Geo-

Eng.2014; 48(1):55-68. Doi:10.22059/
IJMGE.2014.51806i

[15] Ismail Jewan, ZaïriFahmi, Naït-
abdelazizMoussa et al. Computational
modelling of static indentation-induced
damage in glass.
ComputationalMaterials Science. 2008;
42(3): 407-415.DOI:10.1016/j.
commatsci.2007.08.006

[16] Belrhiti Y, Dupre JC, Pop O, et al.
Combination of Brazilian test and digital
image correlation for mechanical
characterization of refractory materials.
Journal of the European Ceramic
Society. 2017; 37(5):2285-2293. DOI:
10.1016/j.jeurceramsoc.2016.12.032

[17] J C Dupré, PDoumalin, H
AHusseini, A Germaneau, FBrémand,
Displacement discontinuity or complex
shape of sample: assessment of accuracy
and adaptation of local DIC approach.
Strain. 2015; 51:391–404. DOI:10.1111/
str.12150

[18] Sakka S, Ben Ayed F, Bouaziz J.
Mechanical properties of tricalcium
phosphate-alumina composites. Mater
Sci Eng.2012; 28: 012028DOI: 10.1088/
1757-899X/28/1/012028

[19] Kuruppu Mahinda D et CHONG
Ken P. Fracture toughness testing of
brittle materials using semi-circular
bend (SCB) specimen. Engineering
Fracture Mechanics. 2012; 91:133-150.
DOI:10.1016/j.engfracmech.2012.01.013

[20] S H Chang, C Lee, S Jeon,
Measurement of rock fracture toughness
under modes I and II and mixed-mode
conditions by using disc-type
specimens, EngGeol. 2002; 66:79–97.
DOI:10.1016/S0013-7952(02)00033-9

[21] FowellRJ, Chen, JF. The third
chevron-notch rock fracture specimen
the cracked chevron notched Brazilian
disk. Proc. 31st U.S. Symp. Rock.
Balkema. Rotterdam. 1990; 295–302.
DOI:10.1016/j.ijrmms.2011.09.019

[22] FowellRJ, XUC. The cracked
chevron notched Brazilian disc test
geometrical considerations for practical
rock fracture toughness measurement.
Int. J. Rock.Mech. Mineral Sci.
Geomech. Abstr. 1993; 30(7):821 – 824.h
ttps://doi.org/10.1016/0148-9062(93)
90029-D

[23] Wang QZ, Jia XM, Kou SQ,
Zhang ZX, Lindqvist P A. More accurate
stress intensity factor derived byfinite
element analysis for the ISRM suggested
rock fracture toughness
specimenCCNBD, Int. J. Rock. Mech.
Min.Sci, 2003; 40:233–241. DOI:
10.1016/S1365-1609(02)00131-4

[24] Iqbal MJ, Mohanty B, Experimental
calibration of stress intensity factors of
the ISRM suggested cracked chevron-
notched Brazilian disc specimen used
for determination ofmode-I fracture
toughness, Int J Rock Mech Min Sci,
2006;43:1270–1276.DOI: 10.1016/j.
ijrmms.2006.04.014

[25] Cherepanov GP. Mechanics of
brittle fracture. New York: McGraw-
Hill; 1979. https://doi.org/10.1007/
BF00037929

[26] Tada H, Paris PS, Irwin GR. The
stress analysis of cracks handbook, 2nd
ed. St Louis: Paris Productions. 1985.

[27] Eftekhari M, Bahbanan A,
Hashemolhosseini H. Extended finite
element simulation of crack propagation
in cracked Brazilian disc, J Min Env.
2015;6(1):95-102.Doi: 10.22044/
JME.2015.365

[28] Shetty DK, RosenfiledAR,
Duckworth, W H, Fracture toughness of
ceramics measured by a chevron notch
diametral compression test, J. Am.
Ceram. Soc, 1985;68 (12):C325 – C327.h
ttps://doi.org/10.1111/j.1151-2916.1985.
tb10135.x

[29] AtkinsonC, SmelserR E, Sanchez J.
Combined mode fracture via the

cracked Brazilian disc test, Int JFract 1982;18):279–91.https://doi.org/10.1007/BF00015688

[30] P Bing, XHui-min, H Tao, A. Asundi, Measurement of coefficient of thermalexpansion of films using digital image correlation method, Polym. Test. 2009;28:75–83. DOI:10.1016/j.polymertesting.2008.11.004

[31] YBelrhiti, A Germaneau, P Doumalin, J CDupré, O Pop, M Huger, TChotard.Characterization of the mechanical behavior of magnesia spinel refractoriesusing image correlation, Proc. of Int. Conf. UNITECR.2013;13:6–41. DOI:10.1111/ijac.12307

[32] L MKachanov, Time of the rupture process under creep conditions, IzvestiyaAkademiiNauk USSR.1958;8: 26–31 (in Russian).

[33] Lemaitre Jean et ChabocheJean-Louis. Mecanique des materiaux solides. Dunod. Mechanics of Solid Materials, Springer, 1985.

[34] Hamza Samir. Etude du comportement en fatigue en compression des biocéramiques (Al_2O_3, ZrO_2) utilisées pour la conception des prothèses ostéo-articulaires. Thèse de doctorat. Université Paul Verlaine-Metz. 2002.https://hal.univ-lorraine.fr/tel-01749598